Superplastic deformation induced by cyclic hydrogen charging

Heeman Choe, Christopher A. Schuh, and David C. Dunand

Citation: Journal of Applied Physics **103**, 103518 (2008);
View online: https://doi.org/10.1063/1.2931003
View Table of Contents: http://aip.scitation.org/toc/jap/103/10
Published by the American Institute of Physics

Superplastic deformation induced by cyclic hydrogen charging

Heeman Choe
School of Advanced Materials Engineering, Kookmin University, Chungneung-dong, Songbuk-ku, Seoul 136-702, Republic of Korea

Christopher A. Schuh
Department of Materials Science and Engineering, Massachusetts Institute of Technology, Cambridge, Massachusetts 02139, USA

David C. Dunand[a)]
Department of Materials Science and Engineering, Northwestern University, Evanston, Illinois 60208, USA

(Received 25 February 2008; accepted 19 March 2008; published online 22 May 2008)

Deformation under the combined action of external stress and cyclic hydrogen charging/discharging is studied in a model material, titanium. Cyclic charging with hydrogen is carried out at 860 °C, which repeatedly triggers the transformation between hydrogen-lean α-Ti and hydrogen-rich β-Ti. Due to bias from the externally applied tensile stress, the internal mismatch strains produced by this isothermal α-β transformation accumulate preferentially along the loading axis. These strain increments are linearly proportional to the applied stress, i.e., flow is ideally Newtonian, at small stress levels (below ~2 MPa). Therefore, after multiple chemical cycles, a tensile engineering strain of 100% is achieved without fracture, with an average strain rate of 10^{-5} s^{-1}, which demonstrates for the first time that superplastic elongations can be achieved by chemical cycling. The effect of hydrogen partial pressure, cycle time, and external stress on the value of the superplastic strain increments is experimentally measured and discussed in light of a diffusional phase transformation model. Special attention is paid to understanding the two contributions to the internal mismatch strains from the phase transformation and lattice swelling.
 [DOI: 10.1063/1.2931003]

I. INTRODUCTION

Processes of cyclic chemical charging/discharging of solid materials are common in a variety of important technologies, ranging from batteries to hydrogen production and storage. During charging, a solute species is introduced and transported through the solid by diffusion, which leads to the production of several types of mismatch stresses, including those from lattice swelling and, frequently, from phase transformations induced by the chemical change. Cyclic charging and discharging then lead to a complex evolution of internal stresses, and these can interact with externally applied stresses to influence the global deformation and damage accumulation in the solid.

Deformation under the combined action of internally generated strain mismatch and external stresses has been studied in other contexts for many years. Specifically, the phenomenon of "internal-stress plasticity" leads to unexpectedly high deformation rates in materials deforming by creep or low-temperature plasticity while internal stresses are produced, and has been widely investigated in a variety of materials (see the review in Ref. 1). When internal mismatch strains are created within a plastically deformable material, they can be biased in the direction of the external stress, which results in a strain increment along this direction, with a magnitude proportional to the biasing stress. If the internal mismatch is constantly regenerated (most commonly, through thermal cycling), then the average strain rate is proportional to the applied stress, which corresponds to an average strain-rate sensitivity of unity, i.e., Newtonian flow. This leads to exceptional flow stability[2] and tensile strains well in excess of 100%, a phenomenon called internal-stress superplasticity.[1]

One common method to repeatably produce internal stresses is to cycle the temperature around a phase transformation temperature, where the two coexisting allotropic phases have different densities. Such "transformation mismatch plasticity" (TMP) induced by thermal cycling has been observed in many allotropic metals and alloys[3] and is particularly well studied in titanium subjected to α-β temperature cycling.[3–8] Dunand and Zwigl[9] first showed that cycles of chemical charging/discharging at constant temperature could also produce TMP. Due to the very high diffusivity of hydrogen, α-Ti can be rapidly alloyed with hydrogen by exposure to a hydrogen-bearing atmosphere, which leads to the formation of the β-Ti phase;[10] upon exposure to vacuum or a hydrogen-free atmosphere, the hydrogen diffuses out of the titanium, which results in a transformation back to the α-Ti phase. Dunand and Zwigl showed that this process, under the simultaneous application of a small external stress, led to irreversible strain increments and average Newtonian flow—the hallmarks of internal-stress plasticity. Because this approach used hydrogen to induce internal stresses at constant temperature, it was named "chemically induced internal-stress plasticity."[10] In that work,[9,10] however, the hydrogen content was much higher than needed for

[a)]Author to whom correspondence should be addressed. Electronic mail: dunand@northwestern.edu.

the transformation, so excess lattice swelling of β-Ti due to hydrogen alloying also occurred, which results in internal stresses due to both reversible transformation and reversible swelling. Reversible swelling without transformation was also found to produce internal-stress plasticity in β-Ti–6Al–4V under stress[11] and strain ratcheting in β-Ti without applied stress,[12] under conditions of cyclic hydrogen charging.

In the present work, we investigate hydrogen-induced TMP with two main goals. First, we demonstrate that superplastic strains (in access of 100%) can indeed be accumulated under conditions of cyclic chemical charging. Second, we aim to experimentally separate phase transformation mismatch from lattice swelling mismatch. We use titanium as a model material and to facilitate comparison with prior literature, but the insights gained here apply more broadly to materials subjected to cyclic chemical charging with a concurrent phase transformation.

II. EXPERIMENTAL PROCEDURES

Cylindrical specimens of unalloyed titanium (Grade 2, from McMaster-Carr, Chicago, IL) were machined with a gauge length of 30.0 mm and gauge diameter of 3.0 mm. The threaded heads had a length of 4.8 mm and a slightly larger diameter of 3.8 mm. Testing was performed in a custom-built creep apparatus,[9] which allows the application of small tensile stresses under a flowing atmosphere. The entering gas could be changed from high-purity 99.999% Ar to a gas mixture of H_2 in Ar. The gas flow rate was constant at 5 l/min, which corresponds to a replacement of apparatus gas volume every 7 s. The cycles consisted of two half-cycles of equal period $t_{1/2}$ (varied from 1 to 10 min) during which the specimens were exposed to pure argon ($p_{H_2}^{min}=0$) and to an Ar/H_2 mixture ($p_{H_2}^{max}>0$). To obtain the average strain increment per cycle, at least five consecutive chemical cycles were performed to ensure a dynamic steady state and to verify reproducibility of the specimen elongation during chemical cycling. Specimen deformation was recorded continuously at the cold end of the lower pull rod by a linear voltage-displacement transducer (LVDT) with a precision of ± 3 μm. The strain increment after the first full cycle was always discarded when calculating an average strain increment, as dynamic equilibrium may not yet have been reached. All tests were performed at 860 °C, a temperature which was maintained within ± 2 °C using a *K*-type thermocouple coated with boron nitride, in contact with the sample. Further experimental details can be found in Refs. 10 and 13.

The microstructure of the CP-Ti was evaluated by optical microscopy on cross sections parallel to the loading axis produced by grinding on SiC paper, polishing with diamond and alumina slurries, and etching for approximately 40 s with a solution of 100 ml distilled water, 2 ml HF, and 5 ml H_2O_2.

III. RESULTS

Figure 1(a) shows the microstructure of CP-Ti in the as-received, undeformed state displaying mostly equiaxed grains ~100 μm in size. Shown in Fig. 1(b) is the microstructure of a sample cooled in the hydrogenated state ($p_{H_2}=200$ Pa). The sample had been deformed at 860 °C under a stress of 1.5 MPa to a strain of 8.1%, following about 60 cycles with $t_{1/2}=1-7$ min. The microstructure consists of β-transformed Widmanstätten plates or laths[14] in a matrix of α-Ti with the majority of elongated β grains aligned along the direction of the applied load (horizontal).

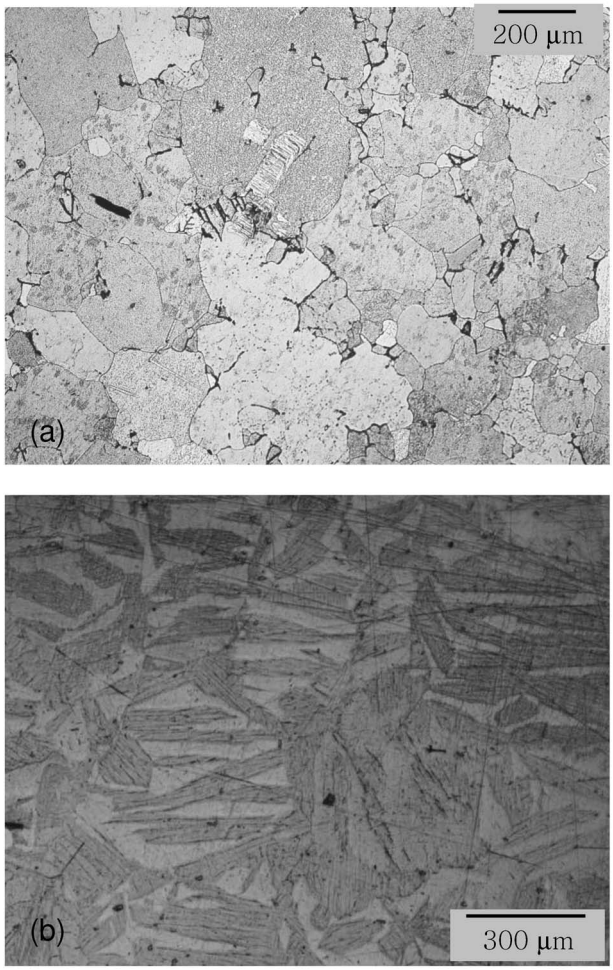

FIG. 1. Optical micrographs of etched commercial purity Ti: (a) in the as-received state and (b) after superplastic deformation through H_2 cycling at 860 °C and 1.5 MPa, then cooling to ambient temperature while charged with hydrogen. The dark phase is the β phase, and the direction of the applied load is horizontal.

Figure 2 shows the stress dependence of the uniaxial steady-state creep rate at 860 °C for H-free α-Ti ($p_{H_2}=0$ kPa) and hydrogenated β-Ti with 14 at. % H (corresponding to the highest hydrogen partial pressure studied, $p_{H_2}=3.8$ kPa) which is well within the β-Ti field [the $\alpha+\beta\rightarrow\beta$ transus corresponding to approximately 3 at. % H or $p_{H_2}=180$ Pa (Ref. 15)]. At a given stress, the creep rate of β-Ti–14%H is approximately an order of magnitude greater than that of α-Ti, as qualitatively expected from the higher diffusion constant of the bcc lattice of β-Ti.[16] The power-law creep exponent for β-Ti–14%H is $n=4.4$, which is identical to that of the α-Ti ($n=4.6$) within error. These values are in agreement with average literature values $n=4.2-4.3$ for α- and β-Ti,[16,17] and the plot in Fig. 2 is in reasonable agreement with a similar plot in Ref. 10. Also shown in Fig. 2 is

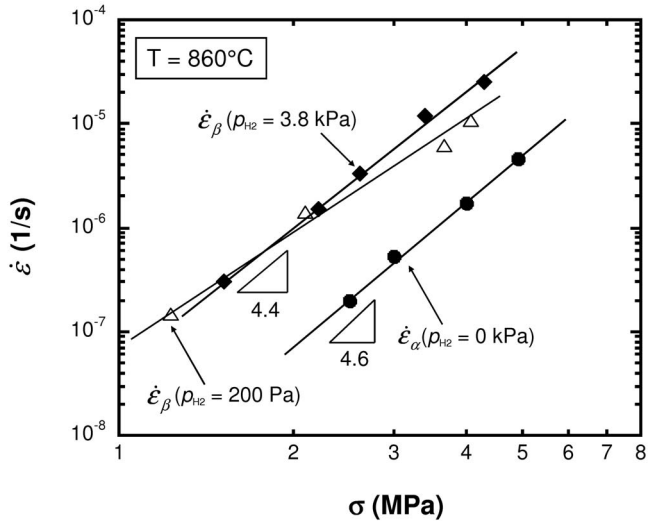

FIG. 2. Stress dependence of the isothermal steady-state creep rate at 860 °C for α-Ti (p_{H_2}=0 kPa) and β-Ti (p_{H_2}=3.8 kPa). Also plotted for comparison is the creep rate of β-Ti at p_{H_2}=200 Pa.

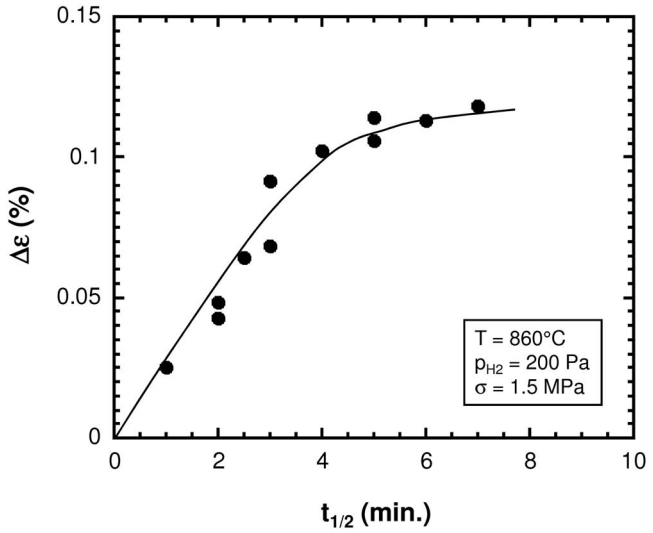

FIG. 4. Creep-corrected strain increment per charging/discharging cycle, as a function of the half-cycle period, for CP-Ti at 860 °C and 1.5 MPa with 200 Pa H_2.

the creep rate of β-Ti–3.2%H (p_{H_2}=200 Pa) with a composition very close to the α-β/β transus line. Within experimental error, there is no difference as compared to the creep rate of the fully hydrogenated β-Ti–14%H sample. This is in agreement with findings by Senkov and Jonas,[18] who showed that the steady-state stress of β-Ti–H samples deformed at a strain rate of 10^{-3} s^{-1} at 920 °C increased only slowly (i.e., by a factor of 1.5) as H concentration increased from 0 to 15 at. %.

Figure 3 depicts the stress dependence of the strain increment $\Delta\varepsilon$ accumulated after chemical cycles at 860 °C with a half-cycle period $t_{1/2}$=10 min at the highest hydrogen partial pressure, $p_{H_2}^{max}$=3.8 kPa. Also shown is the creep strain increment $\Delta\varepsilon_{creep}=t_{1/2}(\dot{\varepsilon}_\alpha+\dot{\varepsilon}_\beta)$ as calculated from data

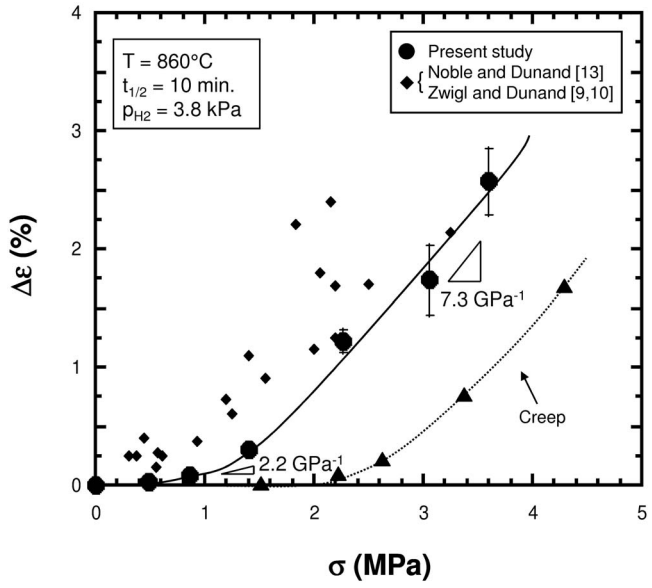

FIG. 3. Strain increment accumulated on each chemical charging/discharging cycle, as a function of the applied stress, for CP-Ti at 860 °C with 10 min half-cycles and 3.8 kPa H_2 (error bars are one standard deviation).

in Fig. 2, accumulated by creep in α- and β-Ti fields for the same time $2t_{1/2}$: the calculated value $\Delta\varepsilon_{creep}$ thus corresponds to the strain increment expected if TMP was not active, and is an upper bound for the strain accumulated during the part of the cycles where hydrogen concentration does not vary significantly (i.e., at the end of both half-cycles). The fact that $\Delta\varepsilon$ from hydrogen cycling is much larger than $\Delta\varepsilon_{creep}$ from creep in Fig. 3 indicates that TMP is the dominant deformation mechanism up to an applied stress of ~4 MPa. Furthermore, the grain structure [Figs. 1(a) and 1(b)] is quite coarse, so that microstructural superplasticity or grain boundary sliding can also be ruled out as a contributing deformation mechanism.

For all further experiments, a baseline hydrogen partial pressure $p_{H_2}^{max}$=200 Pa was chosen, which corresponds to a composition of Ti–3.2%H, very close to the α-β/β transus line. Under these conditions, no swelling of the β-Ti phase can take place. Figure 4 summarizes the results for a series of experiments performed on the sample shown in Fig. 1(b), where $t_{1/2}$ was increased from 1 to 7 min while maintaining the other variables constant ($p_{H_2}^{max}$=200 Pa and σ=1.5 MPa). Figure 4 shows that the strain increment increases nearly linearly with a cycling period up to $t_{1/2}$ =5 min, and remains approximately constant for longer periods. Since the value of $p_{H_2}^{max}$=200 Pa corresponds to a β-Ti–H alloy with the lowest possible H content at 860 °C, it can be inferred from Fig. 4 that 5 min corresponds to the shortest cycle period for which complete α/β/α transformations occur. For shorter cycle periods, the transformation is apparently incomplete, leading to reduced TMP strains. For $t_{1/2}>5$ min, after the sample has been fully charged or discharged, it experiences only a small amount of excess creep deformation at constant composition, resulting in the plateau in Fig. 4.

In Fig. 5, the strain increment $\Delta\varepsilon$ is shown for various applied external stresses from 0.5 to 4 MPa, for $t_{1/2}$=5 min and $p_{H_2}^{max}$=200 Pa (corresponding to complete phase trans-

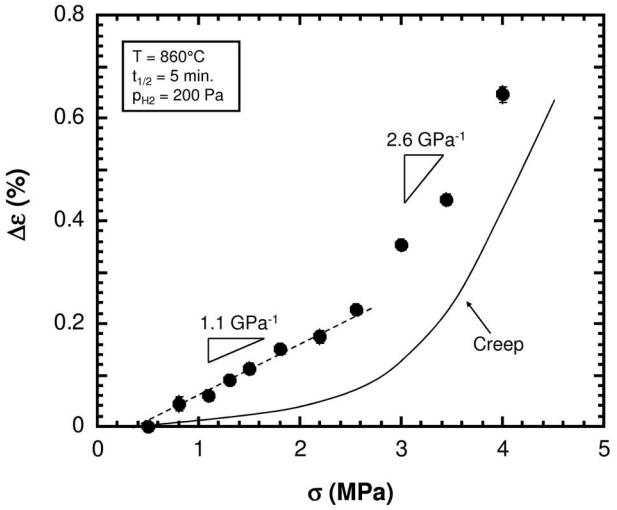

FIG. 5. Stress dependence of the strain increment accumulated on each chemical cycle for CP-Ti at 860 °C with a 5 min half-cycle period at a maximum applied hydrogen partial pressure of 200 Pa.

formations during cycling according to the above discussion of Fig. 4). Near linear behavior is observed for $\sigma = 0.5–2.6$ MPa, with a slope of 1.1 GPa^{-1} and an extrapolated ratcheting strain of about −0.05% at $\sigma=0$. For higher stresses, $\Delta\varepsilon$ increases nearly linearly with an increased slope of 2.6 GPa^{-1}. Also shown in Fig. 5 is the creep strain that would be accumulated in the absence of transformation, $\Delta\varepsilon_{creep}=t_{1/2}(\dot{\varepsilon}_\alpha+\dot{\varepsilon}_\beta)$, as calculated from the data in Fig. 2. It is apparent that the creep strain becomes comparable to the TMP strain at the same stress of ~2.5 MPa where $\Delta\varepsilon$ becomes nonlinear with respect to stress.

Figure 6 summarizes experiments where $p_{H_2}^{max}$ was varied between 50 and 900 Pa, while keeping the stress at σ

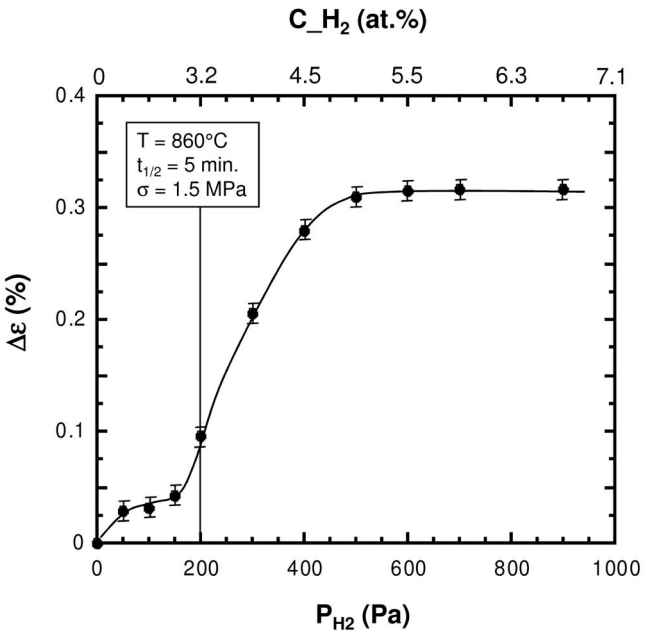

FIG. 6. The plastic strain increment after chemical cycles under a fixed applied stress of 1.5 MPa. The effect of hydrogen partial pressure is shown on the x-axis, which translates via Eq. (4) into an absorbed hydrogen concentration as shown at the top of the figure. For these data, the temperature is 860 °C and the chemical cycles have a half-cycle period of 5 min.

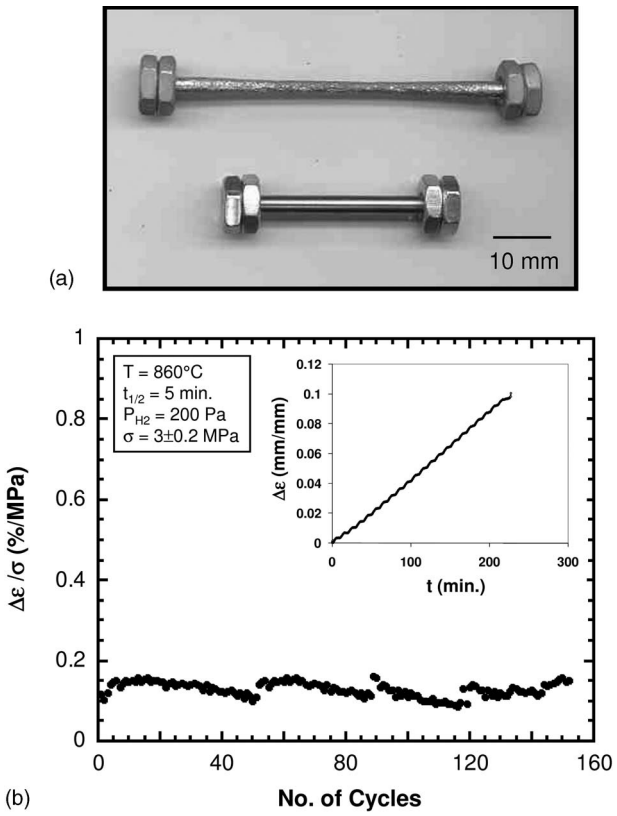

FIG. 7. (a) Photograph of a commercial purity titanium sample deformed to an engineering strain of $e=100.1\%$ after 176 hydrogen cycles at 860 °C, compared to an undeformed sample. The stress was held at 3.0 ± 0.2 MPa during the entire test. Two steel nuts are screwed at each sample head, and provide gripping for the load train. (b) Stress-normalized strain increment and total cumulative strain as a function of the number of cycles for the sample deformed in (a); the average strain rate during the test was roughly constant.

$=1.5$ MPa (in the linear range of Fig. 5) and the half-cycle time at $t_{1/2}=5$ min (which we take to be roughly sufficient for full transformations during cycling at $p_{H_2}^{max}=200$ Pa, based on the results in Fig. 4). Below $p_{H_2}^{max}=200$ Pa, the transformation is incomplete and the strains increase only slightly with $p_{H_2}^{max}$. For $p_{H_2}^{max}=200$ Pa, the hydrogen level is sufficient to induce a complete transformation during cycling, and the strain increment $\Delta\varepsilon=0.1\%$ is similar to those measured in Figs. 4 and 5 for the same conditions ($\sigma=1.5$ MPa and $t_{1/2}=5$ min). For $p_{H_2}^{max}$ between 200 and 500 Pa, the hydrogen level is well above that required to induce the phase transformation, so the sample is subjected to both transformation and excess swelling mismatch strains; over this range, the strain increment increases with $p_{H_2}^{max}$. However, for larger hydrogen partial pressures, i.e., $p_{H_2}^{max}$ between 500 and 900 Pa, the strain increment plateaus at ~0.30%. This is reasonably close to the strain increment for the much higher pressure of $p_{H_2}^{max}=3.8$ kPa (and longer half-cycle time of $t_{1/2}=10$ min), estimated at 0.35% from Fig. 3.

Finally, Fig. 7(a) shows a sample after 176 cycles ($p_{H_2}^{max}=200$ Pa, $t_{1/2}=5$ min, and $\sigma=3.0\pm0.2$ MPa) which accumulated an engineering strain of 100.1%, after which the test was interrupted. Figure 7(b) depicts, for that specimen, the strain increment accumulated on each cycle, as a

function of the test history; here, $\Delta\varepsilon$ is normalized by the applied stress σ, which varied slightly over the course of the experiment. The discontinuities visible in the curve are due to test interruptions and adjustments of the load to maintain an approximately constant stress. The strain increment per cycle is nearly constant throughout the entire experiment, which suggests that there is no long-term change in the structure or accumulation of contaminants from the test atmosphere. For example, we can infer that oxygen contamination is minimal during the test, as oxygen is an α-stabilizer that prevents transformation. Also shown in the inset of Fig. 7(b) is the strain history of the sample for the first 22 cycles. The average strain rate for that segment is $\sim 8\times 10^{-6}$ s^{-1}, which is close to the average value obtained over the entire experiment $\sim 10^{-5}$ s^{-1}. The average strain per cycle in the initial segment is $\Delta\varepsilon=0.45\%$, which is in reasonable agreement with the values reported in Fig. 5, $\Delta\varepsilon=0.30-0.40\%$ for $\sigma=3.0\pm 0.2$ MPa.

IV. DISCUSSION

A. Stress dependence of internal-stress plasticity due to both transformation and swelling

The stress dependence of TMP strain increments $\Delta\varepsilon$ in Fig. 3 can be characterized by the following three regions: (i) for $\sigma<0.8$ MPa, the strain increments are near zero; (ii) for $\sigma=0.8-3.0$ MPa, the strain increments increase linearly, with a slope of ~ 7.3 GPa^{-1}; and (iii) for $\sigma>3.0$ MPa, the strain increments increase more rapidly in comparison to regions (i) and (ii). We identify the following dominant deformation mechanisms for each of these regions: (i) strain ratcheting, (ii) internal-stress plasticity, and (iii) power-law creep. For comparison, we also plot previous data by Zwigl and Dunand[9,10] and Noble and Dunand[13] for experiments performed at the same temperature ($T=860$ °C) and half-cycle time ($t_{1/2}=10$ min) and similar maximal partial pressures ($p_{H_2}^{max}=3.7-4.1$ kPa). The previous data show no ratcheting region (i), a linear region (ii) with a similar slope as for our data, and a nonlinear region (iii) that initiates at a lower stress of approximately 2 MPa.

In all three sets of experiments, it is expected that internal-stress plasticity occurs both due to transformation and swelling mismatch strains.[12] For the high partial pressure of hydrogen $p_{H_2}^{max}=3.8$ kPa, the mismatch produced by lattice swelling of β-Ti is much larger than that produced by the phase transformation. The magnitudes of these mismatches are $(\Delta V/V)_T=0.48\%$ for the α-β transformation and $(\Delta V/V)_S=0.16$ and 1.79% for swelling of α- and β-Ti at 860 °C, respectively.[10,12,19]

We believe that the difference in strain ratcheting and the onset of nonlinearity in Fig. 3 can be attributed to differences in the sample shapes used in these various studies, which strongly affects the diffusion geometry and kinetics, and thus the evolution of the internal mismatch strains. Zwigl and Dunand[9,10] used flat specimens with a gauge of 28–52 mm in length, 5.4–6.0 mm in width, and 1.9–2.6 mm in thickness. Noble and Dunand[13] used cylindrical specimens with a gauge of 20 mm in length and 4 mm in diameter, and with nonthreaded heads of 10 mm in length and diameter. We used here cylindrical samples with a gauge of 30 mm in length and 3.0 mm in diameter, with heads of 4.8 mm in length and 3.8 mm in diameter.

The first systematic difference is in the gauge cross section: ~ 13 mm^2 for the previous studies, and only 7 mm^2 in the present study, so that shorter times can be expected for full hydrogen charging and discharging, and higher composition (and thus mismatch) gradients in the sample. The second systematic difference is in the volume of the heads. Noble and Dunand[13] observed that their relatively large sample head volume could affect the measured strain increments by acting as hydrogen sinks/sources during charging/discharging, which thus affects transformation front geometry and the TMP strains. For this reason, in the present experiments, we reduced the ratio of head to gauge volume, with a value of 0.4, as compared to the very high value of 25 for the previous experiments.[13]

For these reasons, the diffusion profiles in our tests are much more likely to remain perpendicular to the gauge surface, which approximates a semi-infinite axis normal to the hydrogen flux. This condition is much closer to the one experienced in the work of Frary *et al.*,[12] who also found very small (in fact, slightly negative) strain ratcheting under similar hydrogen cycling conditions, which uses cylindrical samples similar to ours. Our results agree with those of Frary *et al.*, and emphasize the potential confounding influence that specimen geometry can have on the diffusion problem, which leads to minor discrepancies among the independent investigations represented in Fig. 3.

B. Effect of half-cycle time upon TMP strains

As noted earlier, the experiments conducted with a low hydrogen pressure of $p_{H_2}^{max}=200$ Pa do not experience complicating effects from swelling of β-Ti, so that the internal-stress plasticity we observe is expected to be due solely to the α-β transformation; deformation occurs by TMP, and should be similar to the well documented TMP of pure Ti subjected to thermal cycling. (We are neglecting the effect of swelling strains in α-Ti because the content of hydrogen dissolved in the α phase is small, the swelling strains are concomitantly small, and this is the stronger of the two phases and can thus be assumed to not plastically deform appreciably.)

With reference to Fig. 4, we recall that for such chemical cycles, with $p_{H_2}^{max}$ at a constant of 200 Pa and at a stress of 1.5 MPa, a half-cycle time of about 5 min was required to achieve the maximum TMP strains, with longer cycles providing essentially no additional strain. This result can be understood by considering the critical half-cycle time for a complete transformation without swelling, which can be estimated as

$$t_{1/2,\mathrm{crit}} \approx \frac{Ta^2}{D}, \tag{1}$$

where D is the diffusion coefficient and a is the sample radius. The parameter T is the dimensionless time required to

fully transform the sample on the slower of the charging and discharging steps, which would be rate limiting for the full cycle. Because the discharging half-cycle requires diffusion of hydrogen out through a thickening outer shell of the lower-diffusivity α phase, we expect that the discharging half-cycle is rate limiting, and use $D_\alpha = 7.3 \times 10^{-5}$ cm^2/s (Ref. 20) in Eq. (1). The kinetics of the moving-boundary phase transformation in a cylinder have been studied in detail in Ref. 21, and the value $T=0.75$ is provided for the current conditions. These values, along with the geometrical parameter $a=1.5$ mm, give an estimated half-cycle time of ~ 3.9 min, which is reasonably consistent with experimental results in Fig. 4 showing that the creep- corrected strain increment starts to level off from $t_{1/2} \sim 4$ min. Later in this paper, we will provide a more detailed numerical model of the phase transformation kinetics, which essentially agrees with the present approximate analysis.

Understanding that the critical $t_{1/2}$ for complete transformation is on the order of ~ 4 min, the remaining features of Fig. 4 follow naturally. The monotonic increase in the strain increment below $t_{1/2} \sim 5$ min is qualitatively expected, as the transformation is only partially complete in that region. The near zero slope for $t_{1/2} > \sim 5$ min further confirms that no additional hydrogen dissolves in the lattice and that no swelling occurs after full transformation is achieved.

C. Stress dependence of TMP strains without swelling

The optimized conditions used in Fig. 5 are expected to minimize lattice swelling mismatch and its associated internal-stress plasticity, while still allowing full TMP to occur. The slopes of the curve are 1.1 GPa^{-1} for lower stress levels (<2.2 MPa) and 2.6 GPa^{-1} for higher stress levels ($2.2 < \sigma < 4$ MPa), respectively, which are much less than those values observed in Fig. 3 (2.2 and 7.3 GPa^{-1}) for the higher partial pressure of hydrogen where both phase transformation and lattice swelling mismatch are involved. In Fig. 5, the slope of 2.6 GPa^{-1} at higher stresses is comparable to the value of 2.3 GPa^{-1} reported in Ref. 4 during thermal cycling of hydrogen-free Ti. However, it is difficult to compare these results directly and, in general, the TMP strains are smaller for chemical cycling than for thermal cycling at a given stress for the following reasons.[13] First, thermal cycling leads to a more rapid transformation, which increases the amount of strain. Second, the transformation temperature of pure Ti is ~ 20 °C lower for chemical cycling, which increases the strength of titanium, thus decreasing the strain increment.[22] Third, chemically induced TMP depends on the motion of a well-defined α/β phase front[21] as compared to the homogeneous nucleation and growth of β grains throughout the α volume in thermally induced TMP. Thus, titanium subjected to chemically induced TMP has highly inhomogeneous stresses localized in regions near the transformation front.

D. Effect of H_2 partial pressure upon TMP strains

It is apparent from Fig. 6 that the strain increment per cycle rose slightly with increasing $p_{H_2}^{max}$ up to ~ 200 Pa where full transformation is achieved, as expected from the increasing volume fraction of transformation. The evolution of the strain increment for $p_{H_2}^{max} > 200$ Pa is complex: increased hydrogen pressure leads to more rapid transformation and thus increased internal strains. Also, higher pressure allows for additional dissolution of hydrogen in β-Ti and the associated lattice swelling strains: the stress gradients due to swelling gradients can cause significant internal-stress plasticity as demonstrated by Schuh and Dunand.[11] Both effects are responsible for the increase in strain increments up to the value of $\Delta\varepsilon = 0.3\%$ in Fig. 6, which is close to the value ($\Delta\varepsilon = 0.35\%$) estimated for $\sigma = 1.5$ MPa at $p_{H_2}^{max} = 3.8$ kPa in Fig. 3.

E. Numerical modeling

To better understand the complex kinetics of the diffusion-induced $\alpha/\beta/\alpha$ phase transformations of Ti, we employed a finite-difference kinetic diffusion model. In this model, an infinite cylindrical specimen was divided into 100 concentric elements of equal thickness in the radial direction, and Fick's second law of diffusion was solved numerically. The diffusion equation was assumed to hold in each phase ($p = \alpha$ or β) present in the system at any given time:[23]

$$\frac{\partial c^p}{\partial t} = \nabla \cdot (D^p \nabla c^p). \tag{2}$$

Equation (2) was also subject to a condition of mass balance at every moving phase transformation front, written below in a one-dimensional form which gives the rate of interface migration, $\partial r_{\alpha/\beta}/\partial t$:

$$\frac{\partial r_{\alpha/\beta}}{\partial t} = \left. \frac{D^\alpha \frac{\partial c^\alpha}{\partial r} - D^\beta \frac{\partial c^\beta}{\partial r}}{c_i^\beta - c_i^\alpha} \right|_{r=r_{\alpha/\beta}}. \tag{3}$$

In these equations, c is the diffusant (hydrogen) concentration, t is the time, D is the diffusion coefficient, r is the spatial coordinate along the radial axis, and $r_{\alpha/\beta}$ is the position of an α/β interface. The boundary conditions for the solution of Eqs. (2) and (3) are an implicit symmetry condition at the cylinder center as well as a fixed surface concentration of hydrogen that is imposed by the thermodynamics of the gas/solid interaction according to Sievert's law:[15]

$$\log p_{H_2} = 2 \log C_{eq} + 7.343 - \frac{4720}{T}. \tag{4}$$

In the present case, the surface concentration is applied as a symmetric square waveform as in the experiments, which alternates between charging [$c > 0$ depending on the pressure in Eq. (4)] and discharging ($c = 0$). Diffusivities from Ref. 20 were assumed to be independent of concentration.

The numerical solution of the above equations requires explicit tracking of the α/β phase boundaries, which was accomplished here by using the fixed-grid method of Crank[23] recast in radial coordinates in Ref. 21. In addition, due to the

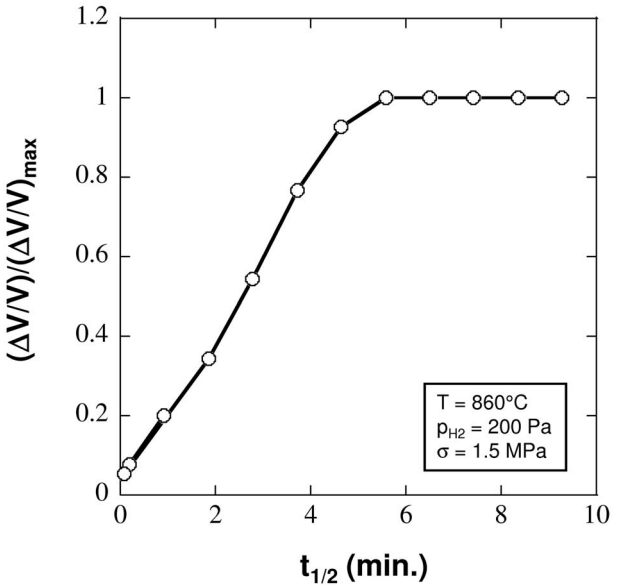

FIG. 8. Model predictions indicating the fraction of volume transformed during dynamic steady-state chemical cycling, plotted as a function of half-cycle time at $p_{H_2}=200$ Pa. The values on the y-axis are normalized by the maximum possible values for a complete phase transformation.

transient nature of the chemical cycling problem, multiple interfaces had to be simultaneously tracked, as a new interface is introduced at the specimen surface on each half-cycle. This complex problem therefore involves multiple interfaces (up to three coexist in the specimen at any time), and these interfaces meet and annihilate occasionally within the specimen. The fixed-grid finite-difference method has been modified to handle these complexities in Ref. 24, and this technique was applied here to the infinite cylinder geometry for the first time. As also described in Ref. 24, it takes several consecutive chemical cycles to achieve a dynamic steady-state condition. For all of the results that follow, a sufficient number of chemical cycles was simulated to reach the dynamic steady state.

We first consider the kinetics of the phase transformation for the idealized experimental conditions in which there is sufficient p_{H_2} to induce a complete transformation, but without causing excess lattice swelling in the β phase. Shown in Fig. 8 is the predicted fraction of volume transformed as a function of half-cycle time for cylindrical samples with a diameter of 3 mm at $p_{H_2}=200$ Pa. The fraction transformed increases with increasing half-cycle time up to ~5.5 min, when complete forward and reverse transformation occurs on every cycle. For longer cycle periods, the transformation is complete relatively earlier, and the sample spends an increasing amount of the total time either completely saturated with hydrogen or free of it. The extra time spent thus cannot contribute to mismatch strain development.

By comparing the simulation results in Fig. 8 with the experimental data in Fig. 4, we first observe that the critical half-cycle time for a complete transformation, $t_{1/2,\mathrm{crit}}$ is in excellent agreement, near ~5 min. This value also compares favorably to our more approximate analysis earlier by using Eq. (1), which gave $t_{1/2,\mathrm{crit}}\approx 4$ min. What is more, if we take the strain increment $\Delta\varepsilon$ as proportional to the volume fraction transformed on each cycle [as is usually literally the case in TMP (Ref. 22)], then we would expect the shape of Fig. 8 to match that of Fig. 4. By comparing these two figures, this expectation is clearly borne out with surprising conformity.

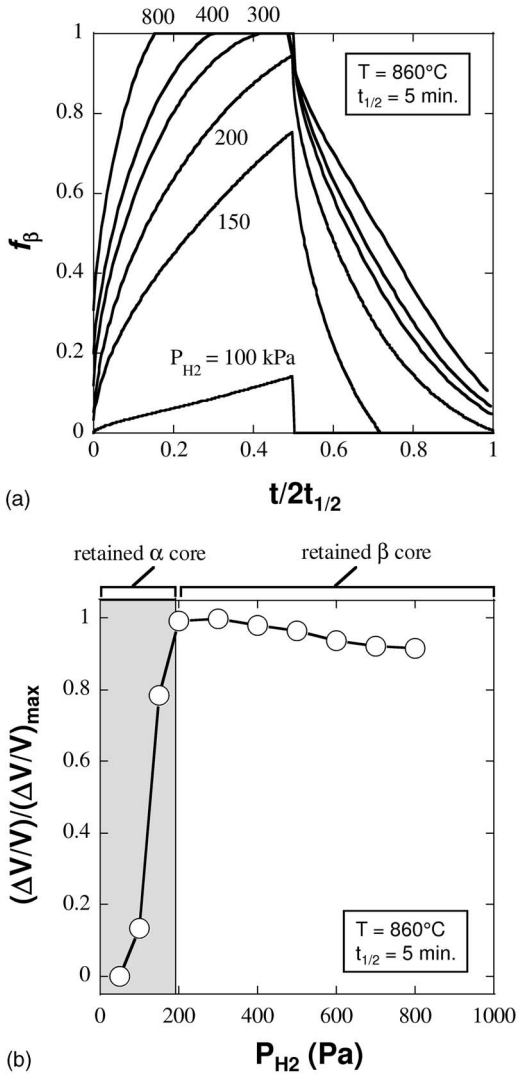

FIG. 9. The effect of hydrogen pressure on diffusional transformation of Ti, which shows (a) predicted hydrogen cycling histories for CP-Ti at various pressures for a half-cycle time of 5 min, where the volume fraction of the β phase is shown at every time and (b) predicted maximum volume fraction of transformation achieved on each cycle during dynamic steady state; here, the value obtained is normalized to the maximum possible value for a complete transformation. The condition of ~200–300 Pa hydrogen pressure is seen to be "optimal" for a complete phase transformation, and separates incomplete transformations with a retained α core (at lower pressures) from those with retained β (at higher pressures).

We may also gain deeper insight into the more complex chemical cycles with different partial pressures of hydrogen. Predicted transformation histories are shown in Fig. 9(a) for 5 min half-cycles, for a variety of conditions that match those of the experiments in Fig. 6. For this cycle period, a hydrogen pressure of $p_{H_2}\approx 200$–300 Pa provides essentially complete forward and reverse transformations on each cycle. It is interesting to observe that this condition actually represents a sort of "optimum" condition for complete phase transformation. This can be observed more clearly by considering the charging/discharging histories that evolve at pressures above and lower than the optimum at 200–300 Pa.

First, we observe in Fig. 9(a) that low partial pressures (below 200 Pa) lead to a situation in which only the surface of the cylinder experiences significant hydrogen concentration and transforms to the β phase; the center of the cylinder always remains in the α phase. Second, we see that higher partial pressures ($P_{H_2} > 300$ Pa) lead to more rapid transformation during charging, but also introduce substantial excess time during which no transformation occurs and the β phase gets charged with additional hydrogen. At the highest applied partial pressures, the sample becomes so charged with hydrogen that it is unable to fully discharge on the discharging half-cycle. Thus, access to more hydrogen on charging leads, somewhat counterintuitively, to incomplete transformation on every cycle, and there is always a portion of the center of the sample that remains in the β phase.

The results from Fig. 9(a) are summarized in Fig. 9(b), where the maximum transformed volume fraction achieved on each full cycle during steady-state cycling is plotted as a function of hydrogen partial pressure. As noted above, the condition of $P_{H_2} = 200-300$ Pa is essentially an optimum condition achieving the most transformation, with pressures both above and below this range leading to incomplete transformation. A vertical boundary line is presented to distinguish between the two situations described above: at low partial pressure, transformation is incomplete and a α-Ti core remains untransformed within the sample, and (ii) at higher pressures, a β-Ti core remains in the center of the sample.

The results in Fig. 9(b) explain the trends measured in our experiments of Fig. 6. First, below $P_{H_2} = 200$ Pa in Fig. 6, only a very small amount of strain was evolved on each cycle. According to Fig. 9(b), under these conditions, the center of the specimen remains in the strong α phase; in this situation, most of the strain accommodation must be accomplished through elastic distortion of the α core, which is reversible; only small plastic strain increments are possible in this condition. At ~200 Pa in Fig. 6, we see a rapid rise in the plastic strain increments, which matches well with the threshold denoted in Fig. 9(b) for a complete transformation. Finally, for higher pressures, the strain increments rise to very high values in Fig. 6, almost certainly due to the additional swelling mismatch strains produced in the β-Ti core, which are more important than the small decrease in transformation strains associated with the decrease in fraction transformed shown in Fig. 9(b). From this analysis, and with reference to Fig. 6, we estimate that the swelling mismatch strain can account for the majority of the plastic strain increments when the partial pressure exceeds about 400 Pa.

V. CONCLUSIONS

We have studied the deformation of commercial purity titanium subjected to reversible hydrogen charging, under conditions where the hydrogen triggers the α/β phase transformation. We find that not only the phase transformation but also lattice swelling due to hydrogen absorption leads to pronounced internal stresses. When small external stresses are also applied during cyclic hydrogen charging, the phenomenon of "internal-stress plasticity" is observed, whereby strain is preferentially accumulated along the axis of the external stress, and the average strain rate along that axis follows a Newtonian flow law. Because of the inherent stability of Newtonian flow, such chemical cycling permits superplastic elongations to occur; we recorded a total engineering strain of 100.1% without failure. To the best of our knowledge, this is the first time that superplasticity induced by cyclic chemical charging has been documented.

We designed our experiments to explore the effect of applied stress, hydrogen partial pressure, and cycling period on the resulting deformation. Our aim was specifically to understand the conditions required to induce a complete phase transformation, and to separate the effects of the transformation and the excess lattice swelling induced by overcharging the β phase after transformation. To assist in understanding the complex diffusion/transformation problem under cyclic charging conditions, we adapted a numerical moving-boundary diffusion model. This model revealed that a pressure of ~200 Pa would lead to complete transformations for cycles of about 5.5 min in duration, at 860 °C for 3 mm diameter rods. Shorter cycles or lower pressures led to incomplete transformation and retained rigid α phase that could sustain load without much deformation. Longer cycles or higher pressures led to overcharging of the β phase with excess hydrogen, a large contribution from lattice swelling, and very high levels of deformation on each cycle. These predictions matched our experimental results quite accurately. The present results provide general guidelines for the design of chemical cycles that can minimize unwanted deformation of structures subjected to cyclic chemical charging.

ACKNOWLEDGMENTS

This study was supported by NSF under Grant No. DMR-9987593. H.C. also acknowledges partial support from the new faculty research program 2007 of Kookmin University in the Republic of Korea.

[1] T. G. Nieh, J. Wadsworth, and O. D. Sherby, *Superplasticity in Metals and Ceramics* (Cambridge University Press, Cambridge, 1997).
[2] C. Schuh and D. C. Dunand, Acta Mater. **49**, 199 (2001).
[3] G. W. Greenwood and R. H. Johnson, Proc. R. Soc. London, Ser. A **283**, 403 (1965).
[4] C. Schuh and D. C. Dunand, Scr. Mater. **40**, 1305 (1999).
[5] D. C. Dunand and C. M. Bedell, Acta Mater. **44**, 1063 (1996).
[6] N. G. D. Murray and D. C. Dunand, Acta Mater. **52**, 2269 (2004).
[7] Q. Li, E. Y. Chen, D. R. Bice, and D. C. Dunand, Metall. Mater. Trans. A **38**, 44 (2007).
[8] C. Schuh, P. A. Noël, and D. C. Dunand, Acta Mater. **48**, 1639 (2000).
[9] D. C. Dunand and P. Zwigl, Metall. Mater. Trans. A **32**, 841 (2001).
[10] P. Zwigl and D. C. Dunand, J. Mater. Process. Technol. **117**, 409 (2001).
[11] C. Schuh and D. C. Dunand, Acta Mater. **49**, 3387 (2001).
[12] M. Frary, C. Schuh, and D. C. Dunand, Philos. Mag. A **81**, 197 (2001).
[13] C. A. Noble and D. C. Dunand, in *First and Second International Symposia on Superplasticity and Superplastic Forming*, edited by D. G. Sanders and D. C. Dunand (ASM, Metals Park, PA, 2003), pp. 88–95.
[14] ASM-Handbook, *Heat Treatment, Structure and Properties of Nonferrous Alloys* (ASM, Metals Park, OH, 1984).
[15] A. D. McQuillan, Proc. R. Soc. London, Ser. A **204**, 309 (1950).
[16] H. J. Frost and M. F. Ashby, *Deformation-Mechanism Maps: The Plastic-*

ity and Creep of Metals and Ceramics (Pergamon, New York, 1982).
[17]C. Schuh and D. C. Dunand, Scr. Mater. **45**, 1415 (2001).
[18]O. N. Senkov and J. J. Jonas, Metall. Mater. Trans. A **27**, 1869 (1996).
[19]H. E. McCoy, Trans. ASM **57**, 743 (1964).
[20]R. J. Wasilewski and G. L. Kehl, Metallurgica **50**, 225 (1954).
[21]C. Schuh, Metall. Mater. Trans. A **31**, 2411 (2000).
[22]C. Schuh and D. C. Dunand, Acta Mater. **46**, 5663 (1998).
[23]J. Crank, *The Mathematics of Diffusion* (Oxford University Press, Oxford, 1989).
[24]C. A. Schuh, J. Appl. Phys. **91**, 9083 (2002).